Published in final edited form as:
Cancer Res. 2008 July 15; 68(14): 5678–5688. doi:10.1158/0008-5472.CAN-07-6589.

Vimentin filaments support extension of tubulin-based microtentacles in detached breast tumor cells

Rebecca A. Whipple[1], **Eric M. Balzer**[1,2], **Edward H. Cho**[1,2], **Michael A. Matrone**[1,2], **Jennifer R. Yoon**[1,2], and **Stuart S. Martin**[1,2,3]

[1] University of Maryland School of Medicine, Marlene and Stewart Greenebaum Cancer Center, Department of Physiology, Baltimore, MD 21201

[2] Graduate Program in Life Sciences

Abstract

Solid tumor metastasis often involves detachment of epithelial carcinoma cells into the vasculature or lymphatics. However, most studies of cytoskeletal rearrangement in solid tumors focus on attached cells. In this study, we report for the first time that human breast tumor cells produce unique tubulin-based protrusions when detached from extracellular matrix. Tumor cell lines of high metastatic potential show significantly increased extension and frequency of microtubule protrusions, which we have termed tubulin *microtentacles* (mcTN). Our previous studies in nontumorigenic mammary epithelial cells showed that such detachment-induced microtentacles are enriched in detyrosinated α-tubulin. However, amounts of detyrosinated tubulin were similar in breast tumor cell lines, despite varying microtentacle levels. Since detyrosinated α-tubulin associates strongly with intermediate filament proteins, we examined the contribution of cytokeratin and vimentin filaments to tumor cell microtentacles. Increased microtentacle frequency and extension correlated strongly with loss of cytokeratin expression and upregulation of vimentin, as is often observed during tumor progression. Moreover, vimentin filaments coaligned with microtentacles, while cytokeratin did not. Disruption of vimentin with PP1/PP2A-specific inhibitors significantly reduced microtentacles and inhibited cell reattachment to extracellular matrix. Furthermore, expression of a dominant negative vimentin mutant disrupted endogenous vimentin filaments and significantly reduced microtentacles, providing specific genetic evidence that vimentin supports microtentacles. Our results define a novel model in which coordination of vimentin and detyrosinated microtubules provides structural support for the extensive microtentacles observed in detached tumor cells and a possible mechanism to promote successful metastatic spread.

Introduction

Successful tumor cell colonization in distant tissues depends on overcoming the selective pressures that are imposed on tumor cells during metastasis (1). Such pressures often select for signaling pathways that support tumor cell survival, motility, invasion, and proliferation following release from the primary tumor site (2–4). Under normal conditions, detachment and dissemination of epithelial carcinoma cells into the microvasculature result in apoptosis or necrosis by shearing forces in narrow capillaries (5,6). However, metastatic tumor cells are able to persist through adapted signaling pathways and can tolerate the morphological

3Corresponding author: Bressler Bldg. Rm 10–29, 655 W. Baltimore St., Baltimore, MD 21201, Tel: 410-706-6601, Fax: 410-706-6600, ssmartin@som.umaryland.edu.

alterations in cell shape, plasticity, and deformation that are necessary to re-adhere and extravasate into distant sites (7–9).

Growing evidence has necessitated a re-evaluation of the functional implications that stable microtubules (MT) have in tumor metastasis. We previously reported observations of extensive and motile, MT-enriched membrane protrusions in detached mouse and human mammary epithelial cells, which promote cell-cell adherence as well as reattachment to uncoated and ECM-coated culture surfaces (10). These protrusions are mechanistically-distinct from actin-based invadopodia, filopodia and cilia, and have been termed tubulin *microtentacles* (mcTN) (10). MT-destabilizing agents significantly reduced the frequency with which microtentacles were observed, and impaired both cell-cell interaction and reattachment of cells to surfaces. Interestingly, MT-destabilizing drugs prevent circulating colon carcinoma cells from attaching to the microvascular endothelium *in vivo*, although the precise mechanism is currently unclear (11). Strikingly, actin depolymerization significantly increases binding of circulating tumor cells to the vascular endothelium (11), and also strongly promotes the extension of tubulin microtentacles (10).

The stability of MTs is influenced by the reversible post-translational cleavage of the COOH-terminal tyrosine of full-length α-tubulin, which is termed tyrosinated tubulin (Tyr-tubulin) (12). Through the action of a yet-unidentifed carboxypeptidase, this tyrosine can be removed rapidly *in vivo*, exposing a COOH-terminal glutamic acid residue and forming detyrosinated α-tubulin (Glu-tubulin)(13). Importantly, poor patient prognosis correlates with elevated levels of Glu-tubulin in breast tumors (14), neuroblastomas (15), and prostate tumors (16), but the mechanism by which increased Glu-tubulin affects tumor progression is currently unknown. We have shown that Glu-tubulin levels significantly increase following epithelial cell detachment, and detachment-induced microtentacles are enriched in Glu-tubulin (10). Cytoplasmic microtubules enriched in Glu-tubulin persist for as long as 16h, while microtubules enriched in Tyr-tubulin generally turn over within minutes (13). However, detyrosination does not directly stabilize tubulin polymers, as Tyr-tubulin and Glu-tubulin polymerize identically *in vitro* (17). Rather, detyrosinated MT associate preferentially with more resilient cytoskeletal components (18), such as the vimentin intermediate filament (IF). This candidate type III IF protein displays anterograde movement toward the plus-ends of MTs (19). Light and electron microscopy also demonstrate that IFs and MTs run parallel in close proximity (20).

Given our recent findings that nontumorigenic mammary epithelial cells display tubulin microtentacles following detachment (10), we explored the occurrence of MT-based microtentacles and MT-associated cytoskeletal proteins in a panel of human breast carcinoma cells. We report for the first time that vimentin-expressing, invasive breast carcinomas display a comparatively higher frequency of tubulin microtentacles following detachment than non-vimentin expressing, non-invasive cell lines. Microtentacle preservation following detachment indicates that vimentin coaligns with Glu-tubulin in microtentacles, while cytokeratin does not. Time-lapse video shows that membrane microtentacles are rapidly disrupted by treatment with PP1/PP2A inhibitors that disassemble vimentin, decreasing microtentacle frequency and impairing reattachment of vimentin-expressing tumor cells. Finally, a dominant-negative vimentin mutant disrupts endogenous vimentin filaments and reduces microtentacles, demonstrating a direct role for vimentin assembly in the mechanism underlying breast tumor microtentacles.

Materials and Methods

Cell Culture

MCF10A human mammary epithelial cells of low passage were grown in DMEM/F12 (Gibco) supplemented with 5% horse serum, insulin (5μg/ml), EGF (20ng/ml), hydrocortisone (500ng/ml). SkBr3, Bt20, MDA-468, Hs578t, MDA-MB-436 were maintained in DMEM (Gibco) while ZR75-1 and HCC1395 were maintained in RPMI (Gibco), both supplemented with 10% bovine calf serum at 37°C in 5% CO_2. MDA-MB-157 were maintained in L-15 (Gibco) supplemented with 10% fetal bovine serum (FBS) at 37°C without CO_2. TIB-131 hybridoma cells that secrete a PAN-intermediate filament antibody (21) were maintained in DMEM supplemented with 10% hybridoma-qualified FBS, sodium pyruvate (1.0mM) at 37°C in 10% CO_2. Sequential adaptation in Hybridoma Serum-Free media (Gibco) was used to subculture cells to minimal serum level for antibody isolation. All cell lines were obtained by American Type Culture Collection (Manassas, VA), and all media was supplemented with penicillin-streptomycin(100 μg/ml each), and L-glutamine (2 mmol/L).

Vimentin Expression Constructs and Transfection

Human vimentin was cloned into the N-terminal eGFP pReceiver-M29 expression vector (Genecopoeia, Germantown, MD). The truncated vimentin was generated by restriction at the internal vimentin *Xho I* site (position 403) and re-ligating the 5′ overhang with a flanking *XhoI* site at the C-terminal multiple cloning site. Both the full-length and truncated vimentin were separated on a gel and sequenced.

Transient transfections of membrane targeted AcGFP1-Mem (Clontech, Mountain View, CA) and CMV-pmRFP-Mem (kindly provided by Georges Luftalla and previously described (22)) were used to visualize and score membrane microtentacles in suspended cells via fluorescent microscopy. Co-transfections were performed with the pmRFP-Mem and the N-GFP vimentin constructs in a 1:1 DNA ratio. MCF10A, SkBr3, Bt20, MDA-MB-157 cells were transfected according to manufacturer's protocol with FuGENEHD transfection reagent (Roche, Branchburg, NJ) using a complex ratio of 3μl of FuGENEHD to 2μg of DNA. ZR75-1, HCC1395, MDA-468, Hs578t, and MDA-MB-436 cells were transfected with Exgen500 (Fermentas, Glen Burnie, MD) using complex ratio of 5.3μl of Exgen500 to 2μg of DNA.

Validated double-stranded siRNA oligonucleotides for human vimentin (5′-CTGGCACGTCTTGACCTTGAA- 3′) and a conjugated Alexa Fluor 488 non-silencing control were purchased from Qiagen (Germany). MDA-MB-436 cells were transfected with HiPerfect (Qiagen, Germany) with 5nM of siRNA. Western blot analysis and immunofluorescence was performed 4, 5, 6d post-transfection. For microtentacle scoring at 6d post siRNA transfection, MDA-MB-436 cells were split 4d post-transfection into optimal confluency conditions for GFP-Mem transfection.

Live Cell Imaging and Membrane Microtentacle Scoring

Cells were trypsinzed at ~80% confluency after 24h expression and resuspended in serum/phenol red (PR)-free media over ultra-low attachment plates in the presence or absence of 5μM Latrunculin-A (LA) (BioMol, Plymouth Meeting, PA) for 1h. For microtentacle scoring involving phosphatase inhibitor treatment, MCF10A and MDA-MB-436 were pretreated with either 1μM okadiac acid (OKA) (Sigma, St. Louis, MO) or 5nM Calyculin-A (CAL-A) (Chemicon, Billerica, MA) in serum-containing media for 1h and resuspended in serum/(PR)-free media in the respective phosphatase inhibitor with or without 5μM Latrunculin-A.

Single cells were scored blindly for microtentacles at 1h in suspension and GFP^+ cells were photographed by fluorescent microscopy. Cells with two or more microtentacles extending greater than the radius of the cell body were scored as positive. Populations of 100 or more GFP^+ cells were counted for each trial. Live and fixed cell images were collected using an Olympus CKX41 inverted fluorescent microscope (Melville, NY) equipped with the Olympus F-View II 12-bit CCD digital camera system and Olympus MicroSuite Five imaging software. Movies of detached cells were captured at one frame every two seconds and are shown with a 5× acceleration.

Differential interference contrast (DIC) images of MDA-MB-436 cells suspended over 35 mm glass bottom dishes (MatTek, Ashland, MA) were acquired using a Zeiss Axiovert 200M motorized microscope equipped with a stage-enclosed incubation system (Incubator XL-3, PeCon, Erbach, Germany). Cells were incubated at 37°C for 10min to allow for transient attachment to anchor cells. Cells that displayed active membrane microtentacles were selected for imaging. Selected cells were imaged over time pre-and post-treament with 1μm OKA or 5nM Cal-A. 3D image stacks were acquired every 3 min for up to 45 min. Zeiss Axiovision software was used for image acquisition and cropping.

Immunofluorescence

To determine cytoskeletal composition of microtentacles observed in suspension, MCF10A and MDA-MB-436 cells were suspended in serum/PR-free media for 30min in the presence or absence 5μM Latrunculin-A. Cells were then fixed in suspension (0.5% glutaraldehyde, 5min.) and gently spun (200rpm, 5min.) onto glass coverslips coated with 1% poly(ethyleneimine) (PEI) solution. Fixative-containing media was aspirated and autofluorescene was quenched using 1mg/ml sodium borohydride solution. For attached cell experiments, MCF10A and MDA-MB-436 on glass coverslips were treated with either 1μM OKA or 5nM Cal-A in serum-free media for 1h at ~80% confluency. Cells were fixed in 3.7% formaldehyde/PBS (10 min., R.T.).

Fixed cells were permeablized (0.25% Triton X-100/PBS, 10 min.), and blocked for 1hr (PBS/5% BSA/0.5% NP40). Immunostaining was performed using mouse monoclonal antibodies vimentin clone V9 (1:1000; Zymed) and PAN cytokeratin clone AE1/AE3 (1:1000; Zymed), and rabbit polyclonal anti-detyrosinated tubulin (Glu; 1:500; Chemicon). Primary incubation was performed overnight at 4°C (PBS/2% BSA/0.5% NP40). Anti-IgG antibodies conjugated to Alexa-594 and Alexa-488 (1:1000; Molecular Probes) were used for secondary detection and Hoescht 33342 (1:5000; Sigma) was used for nuclear staining.

Western Blot

The panel of confluent, untreated cells or specifically, MCF10A and MDA-MB-436 treated in serum/PR-free media at various timepoints in 1μM OKA, 5nM Cal-A, or 30ug/ml cycloheximide were harvested in ice-cold RIPA lysis buffer (50mM Tris-HCl (pH 8.0), 150mM NaCl, 1% NP-40, 0.5% sodium deoxycholate, 0.1% SDS, 1mM phenylmethylsulfonyl fluoride, 1% protease inhibitor cocktail (Sigma, P2714). Lysates were subjected to high-speed centrifugation (14000rpm × 10min) and protein concentration was measured using a Lowry-based assay (Bio-Rad, Hercules, CA). 20μg of total protein was separated by SDS-PAGE on 10% polyacrylamide gels and then transferred to Immuno-Blot PVDF membranes (Bio-Rad, Hercules, CA). Membranes were blocked in 5% milk in TBS with 0.1% Tween for 1hr at room temperature followed by an overnight incubation at 4°C in monoclonal α-tubulin (1:1000; Sigma Chemical), PAN cytokeratin clone AE1/AE3 (1:1000; Zymed), and polyclonal detyrosinated tubulin (1:1000; Chemicon), Vimentin (C-20, Santa Cruz Biotechnology; 1:1000), Vimentin (H-84, Santa Cruz Biotechnology; 1:1000), and PARP (H-250, Santa Cruz Biotechnology; 1:1000), in 2.5% milk in TBST. Monoclonal

PAN-IF isolated from TIB-131 hybridoma cells (1:250) was incubated overnight in 5% milk in TBST. Secondary antibodies to IgG conjugated to horseradish peroxidase were used (1:5000; GE Healthcare, Piscataway, NJ) and visualized using ECL+ chemiluminescent detection kit.

Attachment Assay

MCF10A and MDA-MB-436 cells were grown to confluency in 6-well plates and pretreated in either 1μM OKA or 5nM Cal-A in serum-containing media for 1h. Media and subsequent PBS wash were collected to recover all cells. Cells were trypsinized and resuspended in serum-containing media, collected into respective tube, and pelleted by centrifugation (1000rpm × 5min). Media was aspirated from pellet and cells were gently triturated in fresh serum-containing media containing 1μM OKA or 5nM Cal-A. Cells plated in triplicate in 96-well clear bottom uncoated or laminin-coated (BD Biosciences, San Jose, CA) plates (the attachment plate). Cells were allowed to attach for duration of 15 min, 45 min, 1.5 hr, 3hr, 4hr, 6hr, and 24hr at which point the media was collected into a fresh 96-well uncoated plate (the collection plate). The attachment plate was washed gently with fresh serum-containing growth media without PR and the wash was combined into the collection plate. Fresh growth media was replaced at each timepoint on the original attachment plate. After 24hr, an XTT viability assay was performed on both the attachment and collection plate to quantitatively determine the % of total number of cells plated that had attached at each timepoint. Absorbance was measured using a Biotek Synergy HT Multi-Detection Microplate Reader at 450nm. All values are shown as mean+S.D. of triplicate samples.

Results

Human mammary carcinoma cell lines display morphologically different membrane microtentacles following detachment

We compared the tubulin microtentacles observed in the nontumorigenic MCF10A human mammary epithelial cell line (10), to those in a panel of human breast tumor cell lines. GFP-Mem^{+} cell lines were detached and suspended over ultra-low attachment plates in media deprived of serum and growth factors. Grayscale images collected with fluorescence microscopy were subsequently color inverted for better visualization contrast. Detachment of invasive breast tumor cell lines: Hs578t, HCC1395, MDA-MB-436 and MDA-MB-157 produced unusually long, semi-flexible, and motile microtentacles compared to noninvasive MCF10A, ZR-75-1, Bt-20, SkBr3 and MDA-MB-468 lines, which display relatively short, rigid, and semi-motile microtentacles (Figure 1A and Supplemental Movies 1–3). Our previous research has shown that inhibiting actin polymerization with Latrunculin-A (LA, 5μM) enhances microtentacle frequency, motility and length in both human and mouse mammary epithelial cells following detachment (10). LA similarly increases the length, flexibility and motility of microtentacles in breast tumor cells (Figure 1B and Supplemental Movies 4–6). However, the invasive breast tumor cell lines were clearly able to form dynamic and flexible microtentacles even in the absence of LA treatment. Blinded scoring of microtentacle frequencies (described in Materials and Methods) was conducted in live cells following 30min to 1h in suspension for each of 4 independent trials. Invasive breast tumor cell lines (Hs578t, HCC1395, MDA-MB-436 and MDA-MB-157) all displayed significantly higher microtentacle frequencies ($P<0.05$, t-test) than the noninvasive breast tumor cell lines (Zr-75-1, Bt-20, SkBr3 and MDA-MB-468) or nontumorigenic MCF10A cells (Figure 1C). Microtentacles in both untreated and LA-treated human carcinoma cells can persist at least 48h (data not shown), while MCF10A cells are highly fragmented by late stage apoptosis after 48h of detachment (10).

Vimentin expressing cell lines have more frequent and extensive tubulin microtentacles

While we previously reported that microtentacles are enriched in detyrosinated (Glu) α-tubulin (10), we did not observe significant differences in Glu-tubulin modification or total cellular expression of α-tubulin in the panel of breast tumor cell lines (Figure 1D). These data indicated that Glu-tubulin alone may not account for such distinct morphologies and increased microtentacle frequency in these cell lines. Since microtubules interact with intermediate filaments, we examined cytokeratin and vimentin expression in these cell lines. Western blot analysis (Figure 1D) and indirect immunofluorescence (data not shown) confirmed that non-invasive, epithelioid cell lines ZR-75-1, Bt-20, SkBr3 and MDA-MB-468 homogeneously expressed cytokeratin and not vimentin while moderate- to highly-invasive, fibroblastioid-like cell lines Hs578t, HCC1395, MDA-MB-436 and MDA-MB-157 cells homogeneously expressed vimentin and not cytokeratin. Non-tumorigenic human mammary epithelial cell line MCF10A displayed heterogeneous expression of both vimentin and cytokeratin, with cytokeratin being the dominating intermediate filament in cell monolayers and pronounced vimentin expression at monolayer edges (data not shown). Expression of vimentin is much higher in breast tumor cells which display long and numerous microtentacles, while cytokeratin expression predominated in those cell lines that displayed fewer and shorter microtentacles (Figure 1D).

Vimentin extends into microtentacles

Given the correlation of vimentin expression in those cells that exhibit more extensive and frequent microtentacles, we examined intermediate filament localization with indirect immunofluorescence, finding that vimentin, and not cytokeratin, extends into microtentacles (Figure 2). MCF10A and MDA-MB-436 were used for this and all subsequent experiments, due to the extensive microtentacles of the invasive MDA-MB-436 human carcinoma cell line and the fact that MCF10A cells express both cytokeratin and vimentin. Detached cells were fixed after 30min in suspension in the presence or absence of 5μM LA and centrifuged at low speed onto PEI-coated coverslips to preserve suspended cell architecture for immunofluorescence analysis. LA-treatment enhanced the protrusive effect for immunofluoresence processing as previously described (10). Staining with antibodies against vimentin and a PAN cytokeratin reveal that vimentin is present in microtentacles while cytokeratin is limited to the cell body in MCF10A and weakly diffuse in MDA-MB-436 (Figure 2). Subsequent immunofluorescence of preserved detached cells shows that vimentin and Glu-tubulin co-align in microtentacles of untreated and LA-treated cells suggesting that vimentin may serve to reinforce Glu-tubulin in microtentacles (Figure 3). Extension of microtentacles throughout 3-dimensional space provides challenges to imaging, but confocal imaging allows exclusion of out-of-focus light in rounded cells and highlights the extension of vimentin in microtentacles (Figure 3B).

Disruption of vimentin by phosphatase inhibitors decreases microtentacles

To determine effects of vimentin disruption on morphology and microtentacle frequency, we used two highly selective PP1/PP2A inhibitors that disassemble vimentin IFs via phosphorylation, okadaic acid (OKA, 1μM) and calyculin-A (Cal-A, 5nM),(23,24). MCF10A and MDA-MB-436 lose vimentin organization after treatment with OKA or Cal-A for 1h (Figure 4A). Under normal growth conditions, MCF10A heterogeneously express vimentin in the cell population with intact vimentin extending to the cell periphery (Figure 4A-A). MDA-MB-436 under normal growth conditions homogenously expresses vimentin that extends to the cell periphery with homogenous expression in the cell population (Figure 4A–E). Both cell lines project vimentin filaments from a perinuclear region with concentrated vimentin. Calyculin-A treatment caused fragmentation and a decrease in vimentin that extended to the cell periphery in MCF10A (Figure 4A–B) while a more pronounced effect in MDA-MB-436 was observed with cell rounding, vimentin

fragmentation, and reorganization around the center of the cell body (Figure 4A–F). Treatment with OKA resulted in a more dramatic change in vimentin morphology than Cal-A in MCF10A cells marked by cell rounding and vimentin fragmentation (Figure 4A–D). MDA-MB-436 displayed similar morphological changes with OKA as seen with Cal-A with a slight increase in retraction of the vimentin network to the perinuclear region (Figure 4A–H). Control staining in the absence of serum did not cause noticeable effects on vimentin organization (Figure 4A–B and 4A–F).

To exclude toxicity as a cause for vimentin disruption following Cal-A or OKA treatment, apoptosis was measured by PARP cleavage in MCF10A and MDA-MB-436 cells. No significant PARP cleavage occurred in either MCF10A and MDA-MB-436, even after 6h in Cal-A or OKA (Figure 4B). MCF10A cells remain sensitive to cycloheximide-induced apoptosis, while MDA-MB-436 cells are resistant. An XTT viability assay was performed to confirm that the treatments did not cause apoptosis-independent cell death out to 24h (Figure 4C).

GFP-Mem MCF10A and MDA-MB-436 were pretreated with either Cal-A or OKA for 1h to disrupt vimentin organization, and then suspended in the presence of the corresponding pretreatment for 1h with or without the addition of LA. Blind microtentacle scoring in 3 independent trials demonstrated a significant decrease in microtentacle frequency over the untreated control ($P<0.05$, *t*-test) following vimentin disruption by OKA and Cal-A (Figure 5A) in both MCF10A and MDA-MB-436. LA-enhanced microtentacles are also significantly reduced by combination treatment with OKA+LA or Cal-A+LA ($P<0.05$, *t*-test).

Time-lapse DIC video microscopy shows that untreated MDA-MB-436 cells continue to produce active microtentacles when transiently attached to glass coverslips. The addition of either OKA or Cal-A reduced microtentacle motility and caused retraction approximately 30min post-treatment (Figure 5B, Supplemental Data Movies 7 & 8). These results further indicate that the stability and motion of microtentacles can be inhibited by compounds that affect vimentin phosphorylation.

Disruption of vimentin impairs attachment of vimentin expressing cell lines

Given the role of micotentacles in the reattachment of suspended cells (10), we examined whether vimentin disruption with OKA and Cal-A would also affect reattachment. MCF10A and MDA-MB-436 were pretreated for 1h in OKA or Cal-A, then resuspended in same treatment over uncoated (N=3) or laminin (N=3) tissue culture plates and assessed for cell reattachment. Plots of individual trials (conducted in triplicate) are represented in Figure 5C but the same trend was observed in all trials conducted (Supplemental Figure 1 and 2).

While MCF10A attachment efficiency to either uncoated or laminin-coated surfaces was not significantly affected by Cal-A treatment, attachment was significantly sensitive to treatment with OKA (Figure 6A). This result matches the less-pronounced vimentin disruption in MCF10A cells after Cal-A, as compared to OKA (Figure 4A–B & 4A–D). Interestingly, MDA-MB-436 attachment was significantly impaired by the presence of either Cal-A or OKA (Figure 5C). MDA-MB-436 attachment to uncoated surfaces was impaired (to a greater degree) more significantly at earlier timepoints (15min to 3h) than over laminin at the same early timepoints. The delay in attachment of untreated MDA-MB-436 cells to laminin at early timepoints (15min–1.5h) compared to uncoated plates suggests that a possible adjustment time period is necessary for MDA-MB-436 cells to begin forming permanent attachments and spreading. Cells can become independent of immobilized ECM coatings by depositing new ECM molecules, expressing different ECM receptors, or increasing the ECM receptors (25). Microtentacle-mediated reattachment of suspended cells

to ECM *in vitro* (10) is therefore inhibited by compounds that affect vimentin assembly, and cells expressing high levels of vimentin, such as MDA-MB-436, are comparatively more sensitive to these compounds, potentially indicating a greater dependence of these cell lines on the expressed vimentin.

Dominant negative vimentin mutant inhibits filament assembly and reduces microtentacles

To determine if vimentin directly supports the mechanism underlying microtentacles, we generated a dominant-negative vimentin mutant. With guidance from studies of both *in vitro* vimentin assembly (26) and imaging of vimentin filaments in cells (27), we concluded that isolated expression of an amino-terminal fragment of vimentin lacking the tail region would effectively disrupt vimentin filaments. We engineered a stop codon at amino acid 134 of a GFP-vimentin expression vector, yielding a fragment (GFP-Vim-DN) that contains only the head domain of vimentin and a portion of the rod 1A domain, but lacks any of the tail sequence that is essential for vimentin filament assembly (Figure 6A). Both full-length GFP-vimentin and the GFP-Vim-DN fragment continue to be recognized by an amino-terminal vimentin antibody and GFP antibody, as well as displaying the expected molecular weight shift from fusion with GFP (Figure 6A – inset). Expression of GFP-Vim-DN in three independent invasive breast tumor cell lines (Hs578t, HCC1395 and MDA-MB-436) disrupts endogenous vimentin filaments (Figure 6B). Full-length GFP-vimentin integrates into filaments without disrupting endogenous vimentin. Cotransfection with a membrane-localized red fluorescent protein (pmRFP-Mem) allowed blinded microtentacle scoring in live cells and showed that GFP-Vim-DN significantly reduced microtentacle frequencies in each invasive cell line when compared to full-length GFP-Vim ($P<0.001$, t-test). Reducing vimentin expression with siRNA was not as effective as GFP-Vim-DN at reducing microtentacle frequencies. However, siRNA failed to fully eliminate vimentin, even after 6 days (Supplementary Figure 3). Interestingly, blotting with a pan-intermediate filament antibody indicated that as vimentin levels decreased, a new intermediate filament protein of ~65kDa increased, suggesting a compensatory response to siRNA-mediated vimentin reduction. Such a compensatory mechanism has been proposed for why vimentin knockout mice are viable and phenotypically normal (28), and illustrates the potential limitations of siRNA-mediated downregulation of such an abundant gene with numerous redundant family members. Nevertheless, expression of GFP-Vim-DN disrupted endogenous vimentin filaments within one day and provides genetic evidence that vimentin directly supports the molecular mechanism underlying microtentacles in detached breast tumor cells.

Discussion

Cytoskeletal rearrangements, release of cell-cell contacts, and loss of organized tissue architecture are hallmarks of metastatic progression (29). We previously reported that detached mammary epithelial cells display novel membrane protrusions enriched in detyrosinated α-tubulin; that we have termed tubulin *microtentacles* (mcTN) (10). Continuing our investigation into the occurrence of such microtentacles using a panel of breast carcinoma cells has revealed a marked increase in both microtentacle extension and frequency in more invasive tumor lines. Our data showing colocalization of vimentin with Glu-tubulin in microtentacles, the extensive microtentacles formed in cells with high vimentin expression and the inhibition of microtentacles with dominant negative vimentin or compounds targeting vimentin assembly, all support a model in which structural coordination of Glu-tubulin and vimentin underlie the striking morphological abnormalities we observe in detached breast tumor cells.

Our data also indicate that microtentacles in detached cells are distinct from other actin-based structures in attached cells, such as invadopodia or podosomes (30), which are

inhibited by actin-destablizing agents such as Latrunculin-A or Cytochalasin-D. In contrast, microtentacles are enhanced by actin disruption and appear to become more flexible, motile, and longer (Figure 1B). This supports a model in which inward contraction of the cell's cortical actin counteracts the mechanical forces exerted outward by filaments such as MTs and vimentin, and we are currently examining this repressive role for cortical actin in detail (Balzer, E.M. et al., manuscript submitted). MT-based cilia are characteristically shorter and more highly organized. In addition, MT-based cilia are not known to depend on intermediate filament proteins and their characteristic beat remains unaffected by concentrations of okadaic acid that exceed those we used in our study (31). However, it is possible that tubulin microtentacles were mistakenly identified as such classic cytoskeletal structures in the past. Interestingly, a patient case study reported the occurrence of multiple, "abnormal" microtubule protrusions in an infiltrating mammary ductal carcinoma but remains uncharacterized (32).

Vimentin expression is a marker of the aggressive "basal-cell" subtype of breast tumor (33,34) and upregulation of vimentin predicts metastatic progression and poor patient prognosis (35). Beyond breast cancer, vimentin is an established independent predictor of poor patient prognosis in many tumors, including cervical (36), thyroid (37), hepatocellular (38), pancreatic (39) and renal carcinomas (40). Our results indicate that cell lines with the highest microtentacle counts display reduced expression of cytokeratins and increased vimentin, a change which is also observed during the epithelial-to-mesenchymal transition (EMT) that is associated with tumor progression and poor patient prognosis (41,42). Interestingly, vimentin is also strongly upregulated when tumor cells are exposed to hypoxia (43). Our current evidence supports a direct role for vimentin in the mechanism underlying microtentacles in detached breast tumor cells. Determining how this role for vimentin relates to the additional phenotypic and transcriptional changes that occur during EMT and hypoxia will certainly be an important focus in future studies. In this report, we primarily consider how physical properties of vimentin could support microtentacle extension and potentially provide a selective advantage to tumor cells during metastasis.

Vimentin filaments are far more resilient than microtubules and play an important role in maintaining the integrity and morphology of fibroblastic cells (44). Despite its stability, vimentin can rapidly reorganize in response to phsophorylation. Live cell imaging indicates that microtentacles are comprised of cytoskeletal elements with the structural stability to persist in suspension yet also remain dynamic enough to support rapid movement in response to the cellular microenvironment (Figures 1,5 and Supplemental Movies). Phosphatases associated with vimentin promote filament stability and regulate binding ablility to IF-associated proteins, such as MTs (45). Furthermore, vimentin is rapidly hyperphosphorylated and disassembled after treatment with specific inhibitors of type 1 and 2A phosphatases, providing evidence that vimentin is a major target of PP1 and PP2A activity (23,24).

There is strong evidence that vimentin and stabilized MTs are connected via shared associated proteins such as kinesin motor proteins (46), microtubule associated proteins (MAPs), and intermediate filament associated proteins (IFAPs). Ongoing investigation in our laboratory indicates that kinesins are involved in the microtentacle motility when cells are detached (Yoon, J. et al., manuscript in preparation). Kinesin-dependent crosslinking with vimentin could reinforce stabilized microtubules to allow the plasma membrane deformations that we observe during microtentacle extension. Contraction of the network of cortical actin filaments that lie beneath the plasma membrane usually provides an inward force that counteracts the outward expansion of microtubules from the cell center. The resulting balance of actin and microtubule forces stabilizes cells and is termed *tensegrity* (47). The actin cortex may therefore provide a physical barrier to microtubules, which are

relatively easily broken when encountering compressive stress (48). However, tension and rigidity in the actin cortex decrease when cells are detached, which may partially remove this barrier (49). In addition, compelling recent studies trapping detached breast tumor cells with optical tweezers shows that cell lines with higher metastatic potential have greater flexibility in their actin cortex (50). This inherent weakness in the actin cortex of metastatic breast tumor cells may explain the greater microtentacle extension of invasive breast tumor cell lines, even without actin depolymerization (Figure 1). Given the interest in cytoskeletally-directed therapies for breast cancer, we are currently examining how the counteracting forces of stabilized microtubules and the actin cortex regulate microtentacle extension in breast tumor cells (Balzer, E.M. et al, submitted manuscript).

Based on our results, we propose that upon detachment, vimentin aligns with stable MTs via associated proteins to provide a flexible scaffold to Glu-enriched microtubles which allows microtentacles to protrude at great length from the cell body. The shorter, less frequent microtentacles observed in non-vimentin expressing, less invasive cell lines likely rely on the population of stable MTs but lack the increased resilience and strength of vimentin filaments (48). Disruption of vimentin filaments with either PP1/PP2A inhibitors or dominant-negative mutant vimentin likely promotes the collapse of Glu-MTs and ultimate deformation of the microtentacles.

Research models that involve studying attached cells in culture have limitations when investigating critical steps in the process of metastasis. While we continue to pursue the finctional role of tubulin microtentacles in metastasis, the dramatic morphological differences observed in detached breast tumor cell lines are compelling. Intriguing *in vivo* evidence exists that a yet-unidentified, tubulin-based (not actin-based) mechanism promotes the binding of circulating tumor cells to the vascular endothelium (11). It will therefore be important to determine whether the increased microtentacles in metastatic breast tumor cell lines provide an advantage for successful reattachment and extravasation following dissemination from the primary tumor site. A greater understanding of the foundation and activity of such extensive tubulin microtentacles displayed by invasive carcinoma cells may present an intriguing new target for cancer therapy.

Supplementary Material

Refer to Web version on PubMed Central for supplementary material.

Acknowledgments

This work is supported by a Howard Temin career award (K01-CA096555) and 1R01CA124704-01 from the National Cancer Institute, a Breast Cancer Idea Award from the USA Medical Research and Materiel Command (BC061047) and a Cigarette Restitution Fund Cancer Research Grant (CH 649 CRF) from the State of Maryland Department of Health and Mental Hygiene. We thank Georges Lutfalla for kindly sharing the membrane-localized RFP expression vector.

ABBV

PR	Phenol Red
OKA	Okadaic Acid
Cal-A	Calyculin A
LA	Latrunculin A
CHX	Cycloheximide

Vim	Vimentin
CytoK	Cytokeratin
Glu	Glu (detyrosinated) tubulin
BF	Brightfield
Veh	Vehicle
DIC	Differential interference contrast
GFP	Green Fluorescent Protein
PP1/PP2A	Protein Phosphatase
ECM	Extracellular Matrix

References

1. Steeg PS. Tumor metastasis: mechanistic insights and clinical challenges. Nat Med 2006;12:895–904. [PubMed: 16892035]
2. Wittekind C, Neid M. Cancer invasion and metastasis. Oncology 2005;69 (Suppl 1):14–6. [PubMed: 16210871]
3. Gupta GP, Massague J. Cancer metastasis: building a framework. Cell 2006;127:679–95. [PubMed: 17110329]
4. Wolf K, Friedl P. Molecular mechanisms of cancer cell invasion and plasticity. Br J Dermatol 2006;154 (Suppl 1):11–5. [PubMed: 16712711]
5. Yamauchi K, Yang M, Jiang P, et al. Real-time in vivo dual-color imaging of intracapillary cancer cell and nucleus deformation and migration. Cancer Res 2005;65:4246–52. [PubMed: 15899816]
6. Tsuji K, Yamauchi K, Yang M, et al. Dual-color imaging of nuclear-cytoplasmic dynamics, viability, and proliferation of cancer cells in the portal vein area. Cancer Res 2006;66:303–6. [PubMed: 16397243]
7. Martin SS, Vuori K. Regulation of Bcl-2 proteins during anoikis and amorphosis. Biochim Biophys Acta 2004;1692:145–57. [PubMed: 15246684]
8. Martin SS, Ridgeway AG, Pinkas J, et al. A cytoskeleton-based functional genetic screen identifies Bcl-xL as an enhancer of metastasis, but not primary tumor growth. Oncogene 2004;23:4641–5. [PubMed: 15064711]
9. Martin SS, Leder P. Human MCF10A mammary epithelial cells undergo apoptosis following actin depolymerization that is independent of attachment and rescued by Bcl-2. Mol Cell Biol 2001;21:6529–36. [PubMed: 11533241]
10. Whipple RA, Cheung AM, Martin SS. Detyrosinated microtubule protrusions in suspended mammary epithelial cells promote reattachment. Exp Cell Res 2007;313:1326–36. [PubMed: 17359970]
11. Korb T, Schluter K, Enns A, et al. Integrity of actin fibers and microtubules influences metastatic tumor cell adhesion. Exp Cell Res 2004;299:236–47. [PubMed: 15302590]
12. Barra HS, Arce CA, Argarana CE. Posttranslational tyrosination/detyrosination of tubulin. Mol Neurobiol 1988;2:133–53. [PubMed: 3077315]
13. Webster DR, Gundersen GG, Bulinski JC, Borisy GG. Assembly and turnover of detyrosinated tubulin in vivo. J Cell Biol 1987;105:265–76. [PubMed: 3301867]
14. Mialhe A, Lafanechere L, Treilleux I, et al. Tubulin detyrosination is a frequent occurrence in breast cancers of poor prognosis. Cancer Res 2001;61:5024–7. [PubMed: 11431336]
15. Kato C, Miyazaki K, Nakagawa A, et al. Low expression of human tubulin tyrosine ligase and suppressed tubulin tyrosination/detyrosination cycle are associated with impaired neuronal differentiation in neuroblastomas with poor prognosis. Int J Cancer 2004;112:365–75. [PubMed: 15382060]

16. Soucek K, Kamaid A, Phung AD, et al. Normal and prostate cancer cells display distinct molecular profiles of alpha-tubulin posttranslational modifications. Prostate 2006;66:954–65. [PubMed: 16541425]
17. Khawaja S, Gundersen GG, Bulinski JC. Enhanced stability of microtubules enriched in detyrosinated tubulin is not a direct function of detyrosination level. J Cell Biol 1988;106:141–9. [PubMed: 3276710]
18. Gurland G, Gundersen GG. Stable, detyrosinated microtubules function to localize vimentin intermediate filaments in fibroblasts. J Cell Biol 1995;131:1275–90. [PubMed: 8522589]
19. Yoon M, Moir RD, Prahlad V, Goldman RD. Motile properties of vimentin intermediate filament networks in living cells. J Cell Biol 1998;143:147–57. [PubMed: 9763427]
20. Ball EH, Singer SJ. Association of microtubules and intermediate filaments in normal fibroblasts and its disruption upon transformation by a temperature-sensitive mutant of Rous sarcoma virus. Proc Natl Acad Sci U S A 1981;78:6986–90. [PubMed: 6273900]
21. Pruss RM, Mirsky R, Raff MC, Thorpe R, Dowding AJ, Anderton BH. All classes of intermediate filaments share a common antigenic determinant defined by a monoclonal antibody. Cell 1981;27:419–28. [PubMed: 6086105]
22. Campbell RE, Tour O, Palmer AE, et al. A monomeric red fluorescent protein. Proc Natl Acad Sci U S A 2002;99:7877–82. [PubMed: 12060735]
23. Eriksson JE, He T, Trejo-Skalli AV, et al. Specific in vivo phosphorylation sites determine the assembly dynamics of vimentin intermediate filaments. J Cell Sci 2004;117:919–32. [PubMed: 14762106]
24. Lee WC, Yu JS, Yang SD, Lai YK. Reversible hyperphosphorylation and reorganization of vimentin intermediate filaments by okadaic acid in 9L rat brain tumor cells. J Cell Biochem 1992;49:378–93. [PubMed: 1331124]
25. Mooney DJ, Langer R, Ingber DE. Cytoskeletal filament assembly and the control of cell spreading and function by extracellular matrix. J Cell Sci 1995;108:2311–20. [PubMed: 7673351]
26. Traub P, Scherbarth A, Wiegers W, Shoeman RL. Salt-stable interaction of the amino-terminal head region of vimentin with the alpha-helical rod domain of cytoplasmic intermediate filament proteins and its relevance to protofilament structure and filament formation and stability. J Cell Sci 1992;101 (Pt 2):363–81. [PubMed: 1629250]
27. McCormick MB, Kouklis P, Syder A, Fuchs E. The roles of the rod end and the tail in vimentin IF assembly and IF network formation. J Cell Biol 1993;122:395–407. [PubMed: 8320262]
28. Moisan E, Chiasson S, Girard D. The intriguing normal acute inflammatory response in mice lacking vimentin. Clin Exp Immunol 2007;150:158–68. [PubMed: 17680824]
29. Gotzmann J, Mikula M, Eger A, et al. Molecular aspects of epithelial cell plasticity: implications for local tumor invasion and metastasis. Mutat Res 2004;566:9–20. [PubMed: 14706509]
30. Yamaguchi H, Pixley F, Condeelis J. Invadopodia and podosomes in tumor invasion. Eur J Cell Biol 2006;85:213–8. [PubMed: 16546563]
31. Sutto Z, Conner GE, Salathe M. Regulation of human airway ciliary beat frequency by intracellular pH. J Physiol 2004;560:519–32. [PubMed: 15308676]
32. Reilova-Velez J, Seiler MW. Abnormal cilia in a breast carcinoma. An ultrastructural study. Arch Pathol Lab Med 1984;108:795–7. [PubMed: 6089697]
33. Rodriguez-Pinilla SM, Sarrio D, Honrado E, et al. Vimentin and laminin expression is associated with basal-like phenotype in both sporadic and BRCA1-associated breast carcinomas. J Clin Pathol 2006;60:1006–12. [PubMed: 17105822]
34. Rakha EA, El-Rehim DA, Paish C, et al. Basal phenotype identifies a poor prognostic subgroup of breast cancer of clinical importance. Eur J Cancer 2006;42:3149–56. [PubMed: 17055256]
35. Domagala W, Striker G, Szadowska A, Dukowicz A, Harezga B, Osborn M. p53 protein and vimentin in invasive ductal NOS breast carcinoma--relationship with survival and sites of metastases. Eur J Cancer 1994;30A:1527–34. [PubMed: 7833113]
36. Gilles C, Polette M, Piette J, et al. Vimentin expression in cervical carcinomas: association with invasive and migratory potential. J Pathol 1996;180:175–80. [PubMed: 8976877]

37. Vasko V, Espinosa AV, Scouten W, et al. Gene expression and functional evidence of epithelial-to-mesenchymal transition in papillary thyroid carcinoma invasion. Proc Natl Acad Sci U S A 2007;104:2803–8. [PubMed: 17296934]
38. Hu L, Lau SH, Tzang CH, et al. Association of Vimentin overexpression and hepatocellular carcinoma metastasis. Oncogene 2004;23:298–302. [PubMed: 14647434]
39. Javle MM, Gibbs JF, Iwata KK, et al. Epithelial-mesenchymal transition (EMT) and activated extracellular signal-regulated kinase (p-Erk) in surgically resected pancreatic cancer. Ann Surg Oncol 2007;14:3527–33. [PubMed: 17879119]
40. Kim HL, Seligson D, Liu X, et al. Using tumor markers to predict the survival of patients with metastatic renal cell carcinoma. J Urol 2005;173:1496–501. [PubMed: 15821467]
41. Domagala W, Lasota J, Dukowicz A, et al. Vimentin expression appears to be associated with poor prognosis in node-negative ductal NOS breast carcinomas. Am J Pathol 1990;137:1299–304. [PubMed: 1701960]
42. Willipinski-Stapelfeldt B, Riethdorf S, Assmann V, et al. Changes in cytoskeletal protein composition indicative of an epithelial-mesenchymal transition in human micrometastatic and primary breast carcinoma cells. Clin Cancer Res 2005;11:8006–14. [PubMed: 16299229]
43. Krishnamachary B, Berg-Dixon S, Kelly B, et al. Regulation of colon carcinoma cell invasion by hypoxia-inducible factor 1. Cancer Res 2003;63:1138–43. [PubMed: 12615733]
44. Goldman RD, Khuon S, Chou YH, Opal P, Steinert PM. The function of intermediate filaments in cell shape and cytoskeletal integrity. J Cell Biol 1996;134:971–83. [PubMed: 8769421]
45. Inagaki M, Nishi Y, Nishizawa K, Matsuyama M, Sato C. Site-specific phosphorylation induces disassembly of vimentin filaments in vitro. Nature 1987;328:649–52. [PubMed: 3039376]
46. Prahlad V, Yoon M, Moir RD, Vale RD, Goldman RD. Rapid movements of vimentin on microtubule tracks: kinesin-dependent assembly of intermediate filament networks. J Cell Biol 1998;143:159–70. [PubMed: 9763428]
47. Ingber DE. Tensegrity II. How structural networks influence cellular information processing networks. J Cell Sci 2003;116:1397–408. [PubMed: 12640025]
48. Janmey PA, Euteneuer U, Traub P, Schliwa M. Viscoelastic properties of vimentin compared with other filamentous biopolymer networks. J Cell Biol 1991;113:155–60. [PubMed: 2007620]
49. Heidemann SR, Kaech S, Buxbaum RE, Matus A. Direct observations of the mechanical behaviors of the cytoskeleton in living fibroblasts. J Cell Biol 1999;145:109–22. [PubMed: 10189372]
50. Guck J, Schinkinger S, Lincoln B, et al. Optical deformability as an inherent cell marker for testing malignant transformation and metastatic competence. Biophys J 2005;88:3689–98. [PubMed: 15722433]

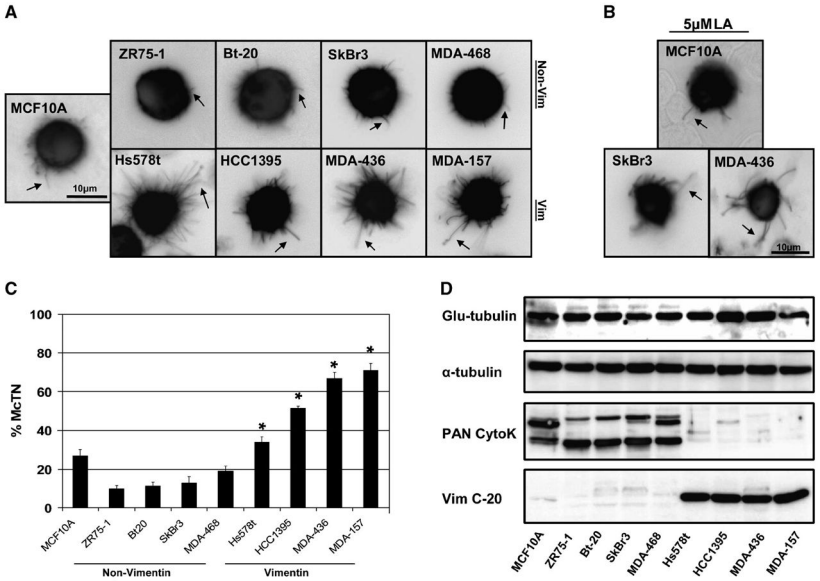

Fig. 1. Microtentacles in detached human breast tumor cell lines

(A) Human mammary epithelial cells (MCF10A) and breast tumor cell lines transfected with GFP-membrane (GFP-Mem) and plated over low-attachment wells display morphologically different extensive membrane microtentacles 30min following detachment (black arrows). Invasive cell lines (HCC1395, Hs578t, MDA-MB-436, MDA-MB-157) exhibit long, flexible microtentacles while non-invasive lines (MCF10A, ZR75-1, Bt-20, SkBr3, MDA-MB-468) display short, rigid microtentacles. (B) Treatment with actin-depolymerizing agent Latrunculin-A (LA, 5μM) enhanced the flexibility and length of observed microtentacles. (C) Populations of live, suspended cells were scored blindly for two or more microtentacles longer than the cell radius. Each bar represents the mean +S.D. for three experiments in which at least 100 single, GFP-Mem$^+$ cells were counted. Vimentin-expressing, invasive cell lines had a statistically-significant higher frequency then non-vimentin expressing, non-invasive cell lines ($P<0.05$, *t*-test, black asterisks). (D) Western blot expression profile of Glu-tubulin, α-tubulin, PAN-cytokeratin, and vimentin indicates that cells with higher microtentacle frequencies express elevated vimentin, lower cytokeratin and Glu-tubulin remains largely unchanged.

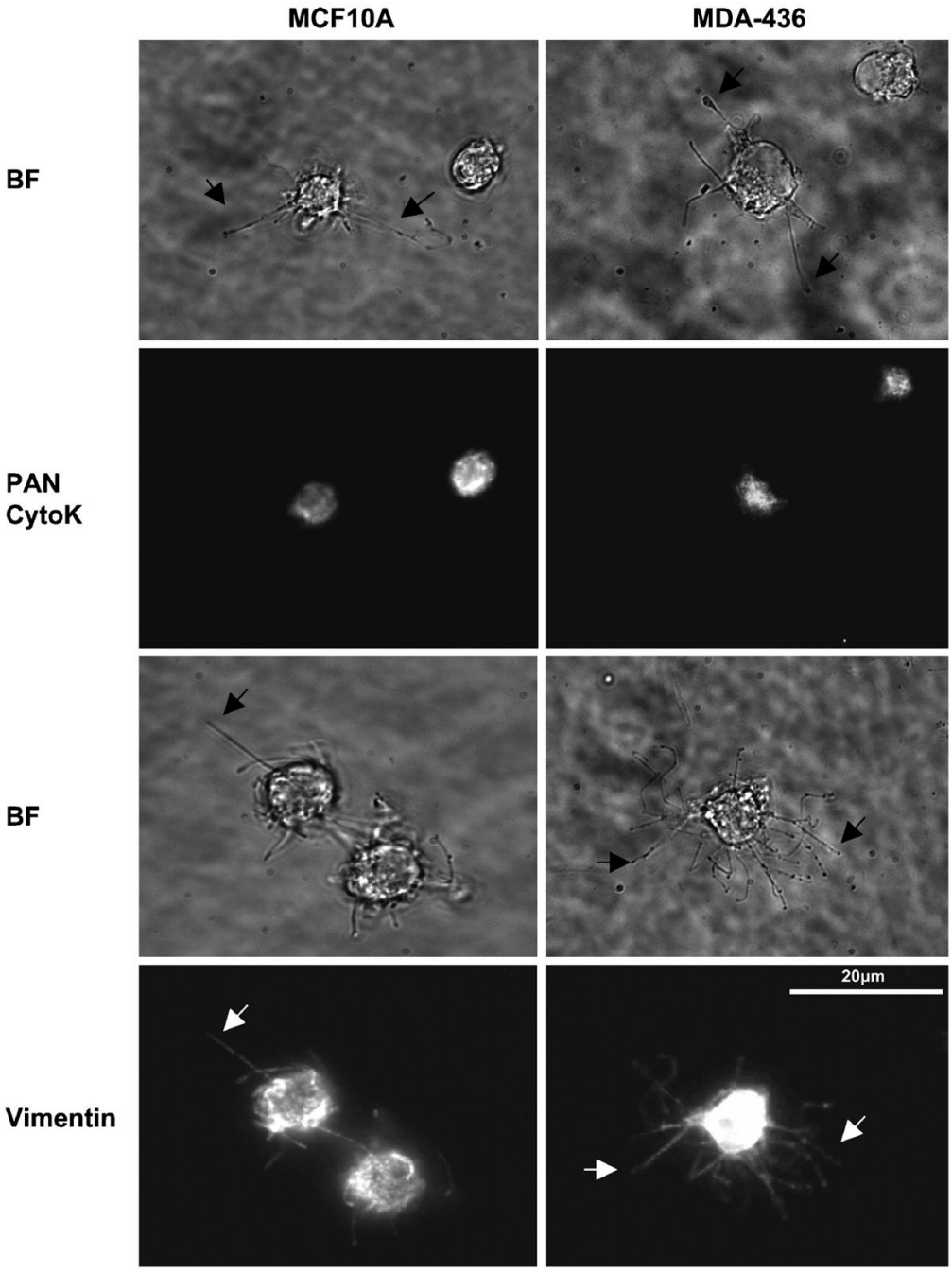

Fig. 2. Vimentin, not cytokeratin, is localized to membrane microtentacles

(A) MCF10A and MDA-436 were suspended for 30min media containing 5μM Latrunculin-A. Cells were fixed in 0.5% glutaraldehyde while in suspension and gently spun onto glass coverslips coated with 1% poly(ethyleneimine) (PEI) solution. Cells were fluorescently stained for vimentin or PAN cytokeratin (CytoK). Microtentacles stain positively for vimentin but not for cytokeratin. Microtentacles can be seen both by phase-contrast (black arrow) and fluorescence (white arrow).

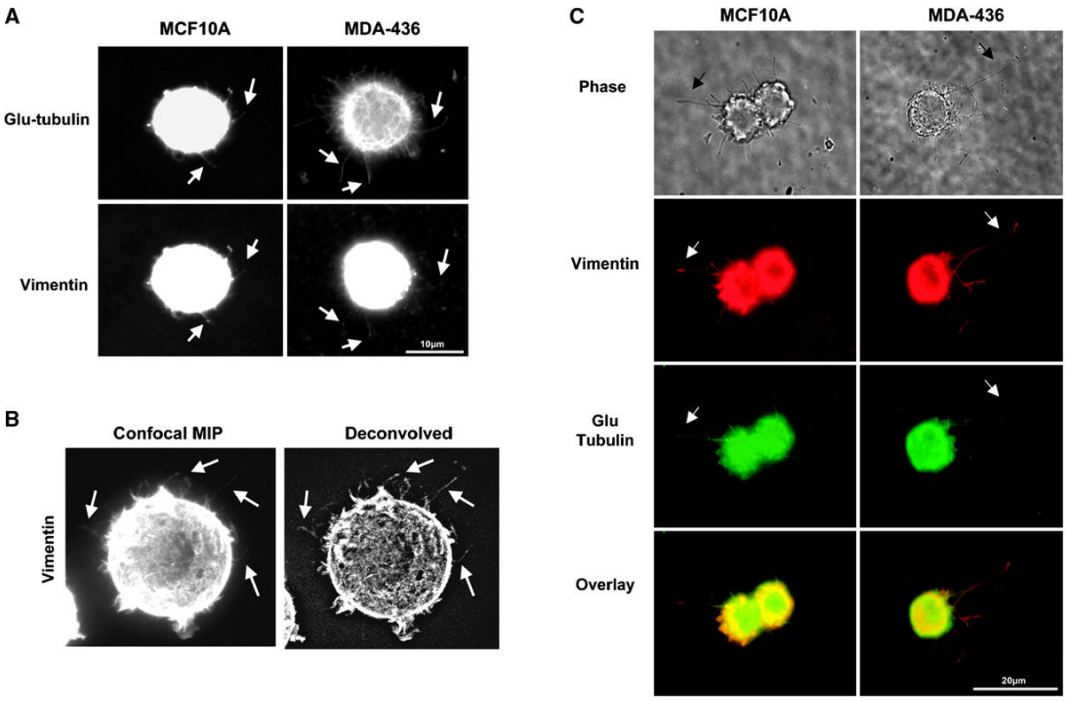

Fig. 3. Vimentin aligns with Glu-tubulin in membrane microtentacles

MCF10A and MDA-436 were suspended for 30min in (A,B) DMEM or (C) media containing 5μM Latrunculin-A. Cells were fixed in 0.5% glutaraldehyde while in suspension and gently spun onto glass coverslips coated with 1% poly(ethyleneimine) (PEI) solution. (A) Immunostaining indicates that both vimentin and Glu-tubulin align in membrane microtentacles. (B) A confocal maximum intensity projection (MIP) of an MDA-MB-436 cell computationally flattens the 3-dimensional structure of the detached cell to allow visualization of microtentacles in different imaging planes. This image and one that has been deconvolved (Slidebook) show clear localization of vimentin in microtentacles (arrows). (C) MDA-MB-436 display significantly longer microtentacles compared to MCF10A. Microtentacles can be seen both by phase-contrast (black arrow) and fluorescence (white arrow).

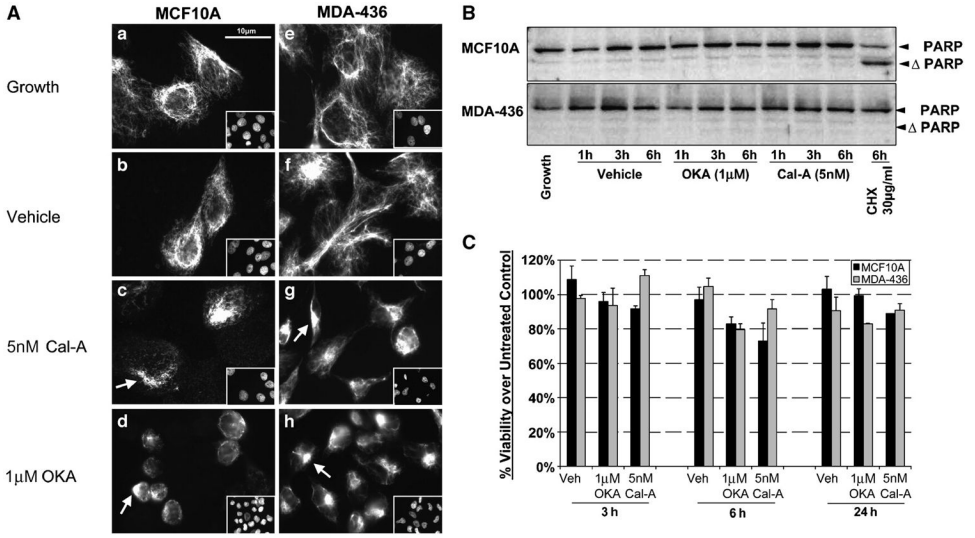

Fig. 4. Inhibitors of PP1/PP2A disrupt vimentin without toxicity

Disruption of vimentin intermediate filaments following 1h treatment in PP1/PP2A inhibitors is observed in attached MCF10A and MDA-MB-436 seeded on glass coverslips. (A) MCF10A and MDA-MB-436 cells grown on glass coverslips were left untreated in growth media (*A, E*); vehicle (0.002% EtOH) treated in DMEM (*B, F*); 5nM calyculin-A (Cal-A) (*C,G*) ; or 1μM okadaic acid (OKA) (*D, H*). Vimentin is heterogeneously expressed in MCF10A while homogeneously expressed in MDA-MB-436 (inset depicts reference DNA stain). Treatment with PP1/PP2A inhibitors causes vimentin fragmentation and retraction to the perinuclear region compared to untreated and vehicle treated cells (white arrows). (B) Cell lysates of MCF10A and MDA-MB-436 treated over for 1h, 3h, and 6hr in Vehicle (0.002% EtOH), OKA (1μM), Cal-A (5nM), and positive control treatment cycloheximide (CHX, 30μg/ml) were immunobloted for PARP cleavage to show minimal degree of apoptosis caused by PP1/PP2A inhibitor treatment. PARP cleavage is observed in the MCF10A positive control but no significant cleavage in presence of PP1/PP2A inhibitors. (C) XTT viability assay shows minimal loss of cell viability via necrosis up to 24h in presence of PP1/PP2A inhibitor treatment.

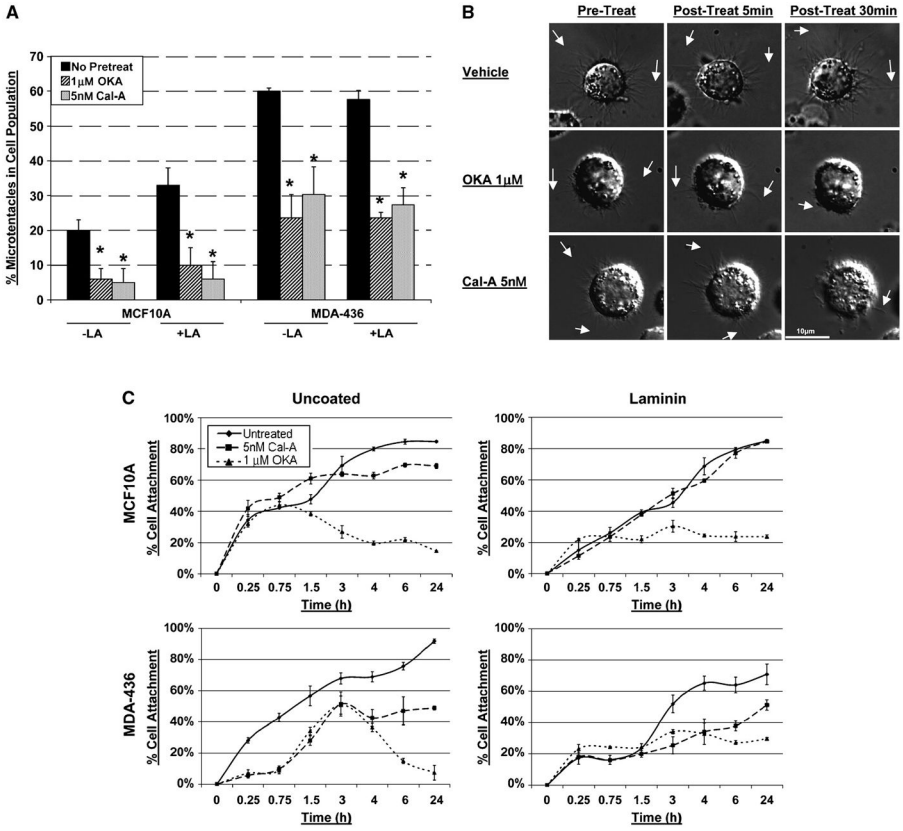

Fig. 5. Vimentin disassembly with PP1/PP2A inhibitors reduces microtentacles and attachment

(A) Transiently transfected GFP-Mem MCF10A and MDA-MB-436 were left untreated (■) or pretreated for 1h in OKA (1μM, ▨) or Cal-A (5nM, ▩) then suspended in DMEM −/+ LA (5μM) in combination with respective pretreatment. Blind microtentacle counts were performed following 30min suspension. Each bar represents the +S.D. for three experiments in which at least 100 GFP-Mem^{+} cells were counted. Pretreatment with both inhibitors and subsequent suspension in the same treatment show a statistically significant reduction in microtentacles in a cell population compared to the untreated counterpart ($P<0.05$, *t*-test, black asterisks). Suspension of cells in the presence of LA also show decrease in microtentacle frequency in combination with PP1/PP2A inhibitors ($P<0.05$, *t*-test, black asterisks). (B) DIC timecourse of transiently attached MDA-MB-436 displaying motile membrane microtentacles captured over 30min timecourse to observe effects of PP1/PP2A inhibitors on microtentacles (white arrows). (C) Disruption of vimentin by PP1/PP2A inhibitors affects cell attachment to surfaces. MCF10A and MDA-MB-436 were left untreated (-◆-) or pretreated for 1h in Cal-A (5nM, -■-) or OKA (1μM, ···▲···). Cells were detached and suspended over uncoated tissue culture plates or laminin coated plates in the presence of the respective PP1/PP2A inhibitor pretreatment. Reattachment efficiency was measured by XTT viability at 24h post-detachment. Values represent mean +S.D. between triplicate wells of the % cells attached in each well. Three independent experiments were performed showing similar attachment curves.

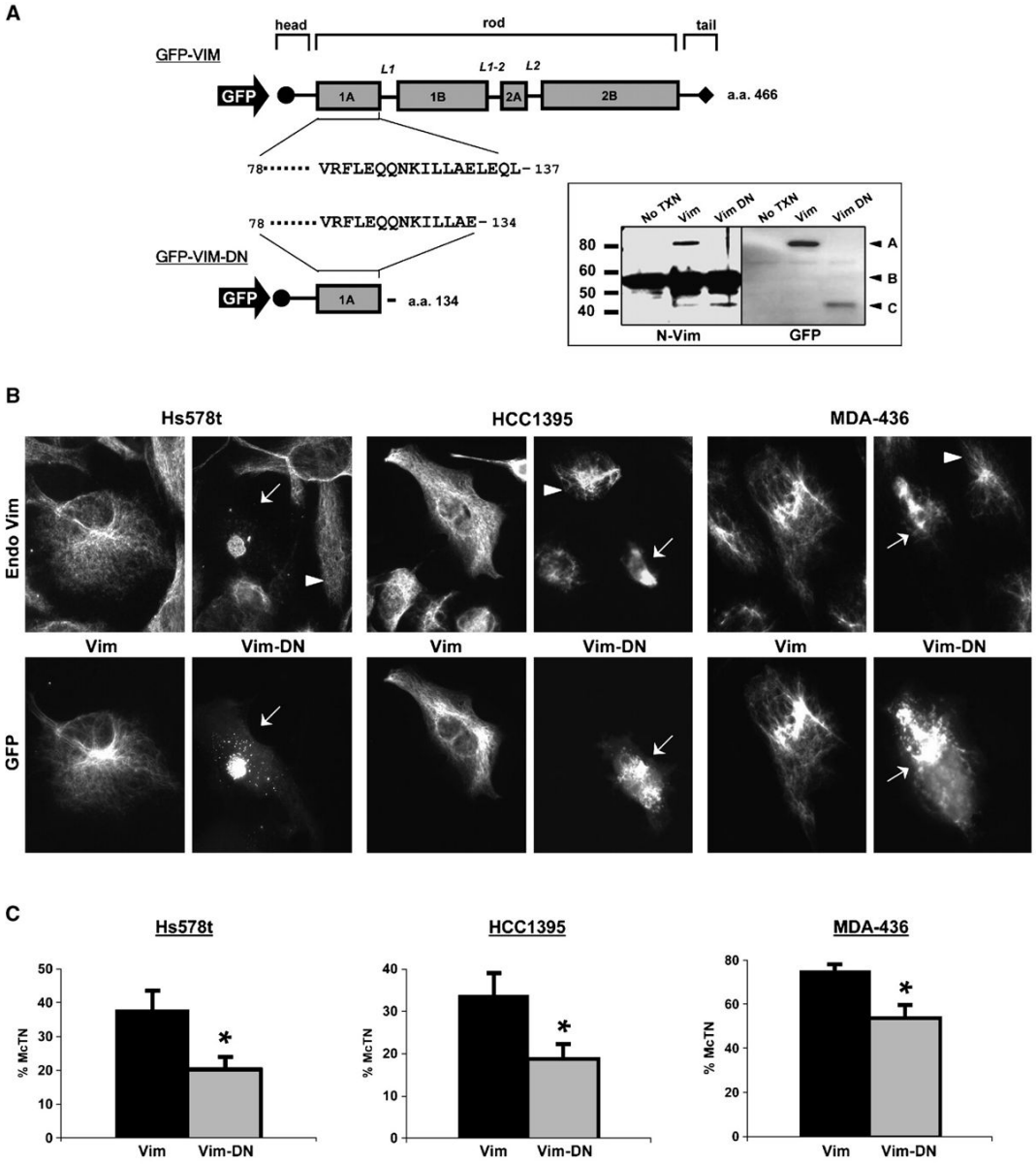

Fig. 6. Dominant negative vimentin (Vim-DN) disrupts filaments and reduces microtentacles

(A) GFP-tagged human vimentin (GFP-Vim) human vimentin was restricted with *Xho I* and religated with a unique *Xho I* site in the C-terminal multiple cloning site to generate a dominant negative form (Vim-DN). The final Vim-DN construct preserves 134 a.a. of the full-length vimentin (466 a.a.) to include the head and highly conserved region of the rod 1A domain. Western blot analysis of Hs578t transfected with the GFP-Vim and GFP-Vim-DN indicates the expression of the truncated GFP-Vim-DN was recognized by both an N-terminal vimentin antibody and GFP antibody [inset - A: GFP Vim (85kD), B: Endo Vim (58kD), C: GFP-Vim-DN (43kD)]. (B) Vimentin expressing cell lines (Hs578t, HCC1395, MDA-MB-436) were transfected with full length vimentin (GFP-Vim) and dominant-negative (GFP-Vim-DN). Matched panels showing localization of the expressed protein (GFP) and endogenous vimentin (Endo Vim) indicate that GFP-Vim-DN disrupts endogenous vimentin in transfected cells (*white arrows*) while surrounding untransfected cells retain their IF network (*white arrowheads*). Expression of full-length GFP-Vim

overlaid with the endogenous IF network indicates that the N-terminal GFP tag Vim is not disruptive. (C) Cells co-transfected with GFP-Vim or GFP-Vim-DN and membrane-targeted RFP (RFP-mem) were suspended in DMEM and blind microtentacle counts were performed following 30min suspension. Each bar represents the +S.D. for at least three independent experiments in which a minimum of 100 RFP-Mem^{+} cells were counted. Expression of the GFP-Vim-DN shows a statistically significant reduction in microtentacles compared to GFP-Vim transfection ($P<0.001$, *t*-test, black asterisks).